

SAURON: An Innovative Look at Early-Type Galaxies

M. Bureau, M. Cappellari, Y. Copin, E.K. Verolme, P.T. de Zeeuw
Sterrewacht Leiden, Niels Bohrweg 2, 2333 CA Leiden, Netherlands

R. Bacon, E. Emsellem
CRAL, 9 Avenue Charles-André, 69230 Saint-Genis-Laval, France

R.L. Davies, H. Kuntschner, R. McDermid
*Physics Department, University of Durham, South Road, Durham
DH1 3LE, United Kingdom*

B.W. Miller
Gemini Observatory, Casilla 603, La Serena, Chile

R.F. Peletier
*Department of Physics and Astronomy, University of Nottingham,
University Park, Nottingham NG7 2RD, United Kingdom*

Abstract. A summary of the SAURON project and its current status is presented. SAURON is a panoramic integral-field spectrograph designed to study the stellar kinematics, gaseous kinematics, and stellar populations of spheroids. Here, the sample of galaxies and its properties are described. The instrument is detailed and its capabilities illustrated through observational examples. These includes results on the structure of central stellar disks, the kinematics and ionization state of gaseous disks, and the stellar populations of galaxies with decoupled cores.

1. Introduction

The physical properties of early-type galaxies correlate with luminosity and environment. The morphology-density relation shows that ellipticals and lenticular galaxies are much more common in clusters than in regions of lower local density (Dressler 1980). Giant ellipticals ($M_B \lesssim -20.5$) are red, have a high metal content, often have boxy isophotes and shallow cusps, and are supported by anisotropic velocity distributions, associated with triaxial shapes (e.g. de Zeeuw & Franx 1991; Faber et al. 1997). Lower-luminosity systems ($M_B \gtrsim -20.5$) are bluer, less metal-rich, have disk-like isophotes and steep cusps, and are flattened by rotation, suggesting nearly oblate shapes (Davies et al. 1983; Bender & Nieto 1990). The mass of the central black hole in spheroids also correlates with the central velocity dispersion (e.g. Gebhardt et al. 2000; Ferrarese & Merritt 2000).

It is unclear to what extent these properties and the correlations between them were acquired at the epoch of galaxy formation or result from subsequent dynamical evolution. Key questions to which SAURON hopes to provide answers include: What is the distribution of intrinsic shapes, tumbling speeds, and internal orbital structure among early-type galaxies? How do these depend on total luminosity and environment? What is the shape and extent of dark halos? What is the dynamical importance of central black holes? What is the distribution of metals, and what is the relation between the kinematics of stars (and gas), the local metal enrichment, and the star formation history?

Progress towards answering these questions requires a systematic investigation of the kinematics and line-strengths of a representative sample of early-type galaxies. The intrinsic shape, internal orbital structure, and radial dependence of the mass-to-light ratio are constrained by the stellar and gas kinematics (e.g. van der Marel & Franx 1993; Cretton, Rix, & de Zeeuw 2000); the age and metallicity of the stellar populations by the absorption line-strengths (Gonzalez 1993; Davies, Sadler, & Peletier 1993). The SAURON project will provide all of these data, and more, for a large and well-defined sample of objects.

2. The Instrument

Long-slit spectroscopy along a few position angles is insufficient to map the rich internal kinematics of early-type galaxies (e.g. Statler 1991, 1994). We thus built SAURON (Spectral Areal Unit for Research on Optical Nebulae), a panoramic integral-field spectrograph optimized for studies of the large-scale kinematics and stellar populations of spheroids (Bacon et al. 2001, hereafter Paper I). SAURON uses a lenslet array and is based on the TIGER concept (Bacon et al. 1995). In its low-resolution (LR) mode, it has a $41'' \times 33''$ field-of-view sampled with $0''.94 \times 0''.94$ lenslets, 100% coverage, and high throughput. In high-resolution (HR) mode, the field-of-view is $11'' \times 9''$ sampled at $0''.27 \times 0''.27$. SAURON simultaneously provides 1577 spectra over the wavelength range 4810–5350 Å, 146 of which are used for sky subtraction. Stellar kinematic information is derived from the Mgb triplet and the Fe lines; the [OIII], H β , and [NI] emission lines provide the morphology, kinematics, and ionization state of the ionized gas. The Mgb, H β , and Fe5270 absorption lines are sensitive to the age and metallicity of the stellar populations. The main characteristics of SAURON are listed in Table 1. Paper I provides a full description of its design, construction, and of the extensive data reduction software we developed. A pipeline called PALANTIR is also described.

3. The Sample

Observing any complete sample which spans a wide range of properties is costly in telescope time, even with SAURON. We therefore constructed a *representative* sample of nearby ellipticals, lenticulars, and early-type bulges, as free of biases as possible, but ensuring the existence of complementary data. We also target some objects with known decoupled kinematics (e.g. Davies et al. 2001). We will combine the SAURON observations with high-spatial resolution spectroscopy of the nuclei, mainly from CFHT/OASIS and HST/STIS, and interpret them through dynamical and stellar population modeling.

Table 1. SAURON's Main Characteristics

Property	Mode	
	LR	HR
Projected size of lenslet	0'94	0'27
Field-of-view	41" × 33"	11" × 9"
Spectral resolution (FWHM)	3.6 Å	2.8 Å
Wavelength coverage	4810–5350 Å	
Number of object lenslets	1431	
Number of sky lenslets	146	
Grism	514 lines mm ⁻¹	
Spectral sampling	1.1 Å pix ⁻¹	0.9 Å pix ⁻¹
Instrumental dispersion (σ)	90 km s ⁻¹	70 km s ⁻¹
Spectra separation/PSF ratio	1.4	2.3
Important spectral features	H β , [OIII], Mg _b , FeI, [NI]	
Calibration lamps	Ne, Ar	
Telescope	William Herschel 4.2-m	
Detector	EEV12 2148×4200	
Pixel size	13.5 μ m	
Efficiency (optics/total)	≈35%/14.7%	

To construct the sample, we first compiled a complete list of ellipticals, lenticulars, and spiral bulges for which SAURON can measure the stellar kinematics. Given the specifications of the instrument, this leads to the following constraints: $-6^\circ \leq \delta \leq 64^\circ$ (zenith distance), $cz \leq 3000$ km s⁻¹ (spectral range), $M_B \leq -18$ and $\sigma_c \geq 75$ km s⁻¹ (spectral resolution). We further restricted the objects to $|b| \geq 15^\circ$ to avoid crowded fields and large Galactic extinctions. All distances are based on a Virgocentric flow model. For galaxies in the Virgo cluster, Coma I cloud, and Leo I group, which we refer to as ‘cluster’ galaxies, we adopted common mean distances based on the mean heliocentric velocity of each group (Mould et al. 1993). For galaxies outside these three associations, which we refer to as ‘field’ galaxies, we used individual distances.

The complete list of galaxies contains 327 objects which we divided into six categories, first separating ‘cluster’ and ‘field’ galaxies, and then splitting each of these into E, S0, and Sa bulges. We then selected the *representative* sample of objects by populating the six resulting ellipticity versus absolute magnitude planes nearly uniformly. The result is 36 cluster galaxies (12 E, 12 S0, and 12 Sa) and 36 field galaxies (12 E, 12 S0, and 12 Sa), as illustrated in Figure 1. By construction, our sample covers the full range of environment, flattening, rotational support, nuclear cusp slope, isophotal shape, etc. It is also large enough to be sub-divided by any of these criteria, and allow a useful comparison of the sub-samples, yet small enough that full mapping with SAURON is possible over a few observing seasons. The 72 galaxies correspond to 22% of the complete sample and, as can be seen from Figure 1, remain representative of it. A more complete description of the sample as well as a listing are available in de Zeeuw et al. (2001, hereafter Paper II). Over two-thirds of the sample have been observed as of September 2001. Completion is expected in April 2002.

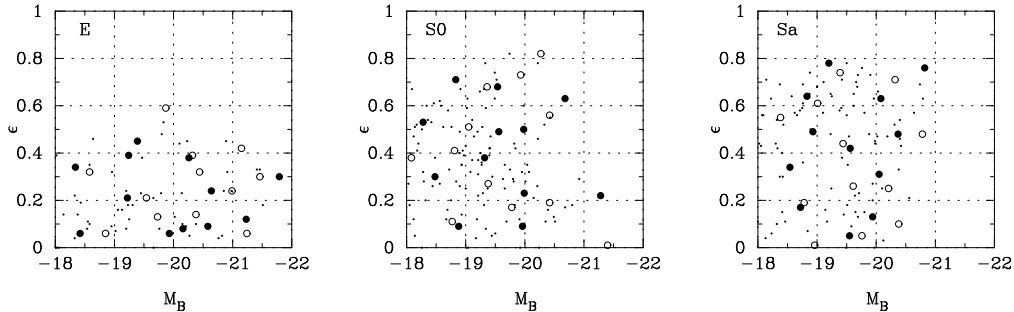


Figure 1. Distribution of E, S0, and Sa galaxies in the SAURON representative sample, in the planes of ellipticity ε versus absolute blue magnitude M_B . Open circles: field galaxies. Filled circles: cluster galaxies. Small dots: remaining galaxies of the complete sample.

4. Stellar Kinematics

Our strategy is to map galaxies to one effective radius R_e , which for nearly half the sample requires only one pointing. For the largest galaxies, mosaics of two or three pointings reach $0.5 R_e$. Each pointing is split into four 1800 s exposures dithered by one lenslet. We reduce the raw SAURON data as described in Paper I and derive maps of the stellar kinematics using the FCQ method (Bender 1990). This provides the mean stellar velocity V , the velocity dispersion σ , and the Gauss-Hermite moments h_3 and h_4 (e.g. van der Marel & Franx 1993).

In this section, we present SAURON stellar kinematics for three objects observed in the LR mode. All show the presence of a central stellar disk, with varying strengths. Other morphologies are illustrated in Papers I and II.

4.1. NGC 3384

NGC 3384 is a large SB0⁻(s) galaxy in the Leo I group ($M_B = -19.6$). It forms a triple on the sky with NGC 3379 and NGC 3389 but there is only marginal evidence for interactions. The light distribution in the central $\approx 20''$ is complex. The inner isophotes are elongated along the major axis, suggesting an embedded disk, but beyond $10''$ the elongation is along the minor-axis (e.g. Busarello et al. 1996). The isophotes are off-centered at much larger radii. NGC 3384 shows no emission lines, remains undetected in HI, CO, radio continuum, and X-ray, but has IRAS detections at 12 and $100 \mu\text{m}$ (e.g. Roberts et al. 1991).

Figure 2 displays the stellar kinematics of NGC 3384 and illustrates a key advantage of SAURON. Integrating the flux in wavelength, the surface brightness distribution of the galaxy is recovered and there is no doubt about the relative location of the measurements. Figure 2 shows that the bulge of NGC 3384 is rotating regularly. The mean velocities increase steeply along the major axis up to $r \approx 4''$, then decrease slightly, and rise again. No velocity gradient is observed along the minor axis. The velocity dispersion map shows a symmetric dumb-bell structure and the h_3 map is anti-correlated with V in the inner parts, revealing an abrupt change in the gradient at $r \approx 4''$ (see also Fisher 1997). All these facts point to the presence of central (and cold) stellar disk in NGC 3384.

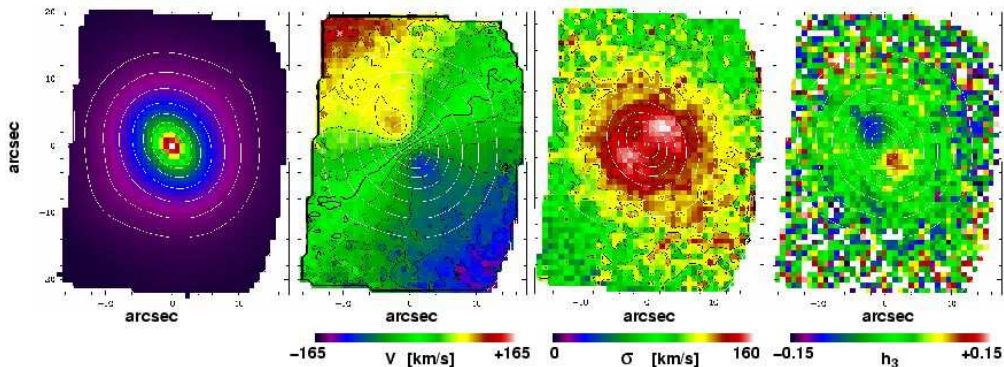


Figure 2. SAURON absorption-line measurements of the SB0 galaxy NGC 3384, based on a single pointing of 4×1800 s. The effective spatial sampling is $0''.8 \times 0''.8$ and the seeing was $\approx 2''.5$. a) Reconstructed total intensity I . b) Mean stellar velocity V . c) Stellar velocity dispersion σ . d) Gauss-Hermite moment h_3 . The Gauss-Hermite moment h_4 displays little variation over the field and is not shown.

4.2. NGC 4526 and NGC 4459

Many other galaxies in our sample show evidence of a central stellar disk. NGC 3623 was discussed in Paper II. Figure 3 shows two other cases where the stellar disk appears to corotate with a central gaseous disk limited by the dust lane (Rubin et al. 1997). NGC 4526 is a highly inclined SAB0⁰(s) galaxy in the Virgo cluster ($M_B = -20.7$). The stellar disk is not readily visible in the reconstructed image, but it is evident in the velocity and velocity dispersion fields. As in NGC 3384, the rotation along the major axis first increases, then decreases, and increases again in the outer parts. However, the extent of the disk is much larger than in NGC 3384. The disk appears almost edge-on, giving rise to an elongated depression across the (hot) spheroid in the velocity dispersion map, and completely overwhelming the central velocity dispersion peak.

NGC 4459 is an S0⁺(r) galaxy ($M_B = -20.0$) also located in Virgo and harbouring a $7.3 \times 10^7 M_\odot$ black hole (Sarzi et al. 2001). The same velocity behavior as in NGC 3384 and NGC 4526 is observed along the major axis (see also Peterson 1978), although the minimum is shallower. The isovelocity contours are also less skewed, either indicating that the disk is seen more face-on or that it is intrinsically thicker (or both). This is supported by the absence of a clear disk signature in the velocity dispersion map.

5. Gaseous Kinematics and Ionization Mechanisms

We now illustrate the scientific potential of the SAURON gaseous data. Paper II describes how the H β , [NI], and [OIII] emission lines are disentangled from the absorption lines by means of a spectral library, and it summarizes the procedures for deriving fluxes and kinematics. Results on the non-axisymmetric gaseous disks in NGC 3377 and NGC 5813 are presented in Papers I and II, respectively.

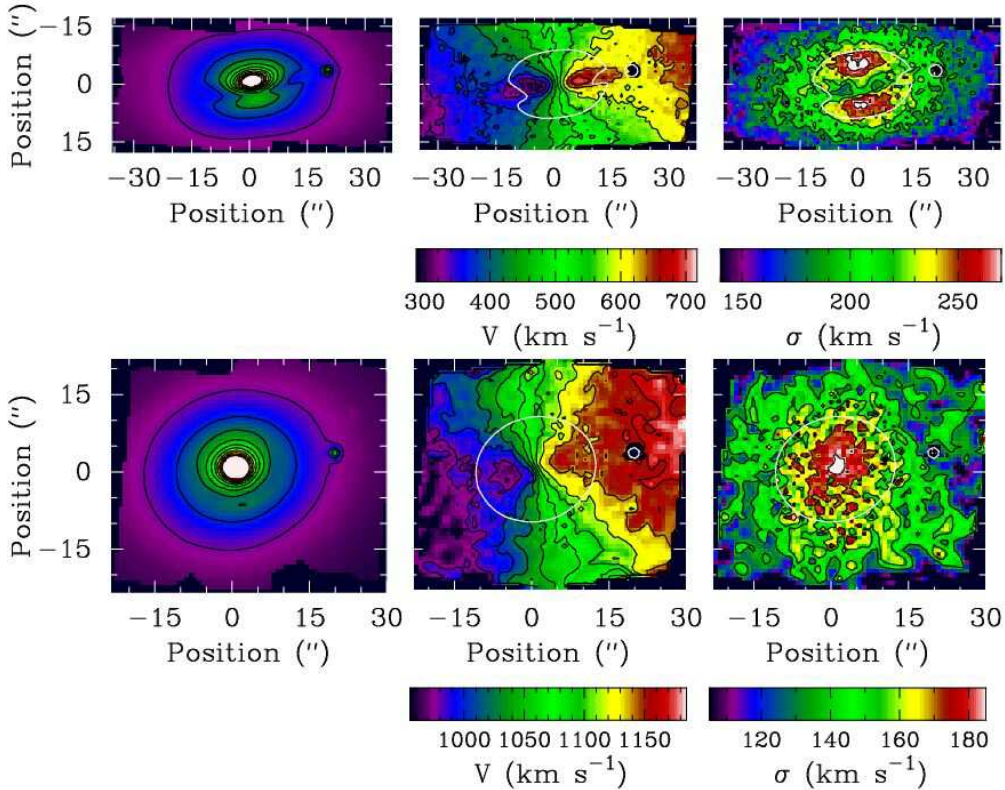


Figure 3. SAURON absorption-line measurements of the SBO galaxies NGC 4526 and NGC 4459, both based on two partially overlapping pointings. Top row: Reconstructed total intensity, mean stellar velocity, and velocity dispersion fields of NGC 4526. Bottom row: Same for NGC 4459. Isophotes are overlaid on all fields as a reference.

5.1. NGC 7742

NGC 7742 is a face-on Sb(r) spiral ($M_B = -19.8$) in a binary system. It is among the latest spirals included in our sample. De Vaucouleurs & Buta (1980) identified the inner stellar ring; Pogge & Eskridge (1993) later detected a corresponding small, bright ring of HII regions with faint flocculent spiral arms. NGC 7742 possesses a large amount of HI, molecular gas, and dust (e.g. Roberts et al. 1991) and is classified as a LINER/HII object (Ho, Filippenko, & Sargent 1997).

Figure 4 shows the [OIII] and $H\beta$ intensity maps, together with the derived velocity and velocity dispersion fields. Most of the emission is confined to a ring coinciding with the spiral arms. $H\beta$ dominates in the ring ($H\beta/[OIII] \approx 7 - 16$) but it is much weaker in the center ($H\beta/[OIII] \approx 1$). Also shown in Figure 4 is a reconstructed image composed of [OIII] and stellar continuum, and a similar image composed of HST/WFPC2 exposures. The SAURON data does not have HST's spatial resolution, but it does show that our algorithms yield accurate emission-line maps. The main surprise comes from the stellar and gas kinematics: the gas and stars within the ring are counter-rotating.

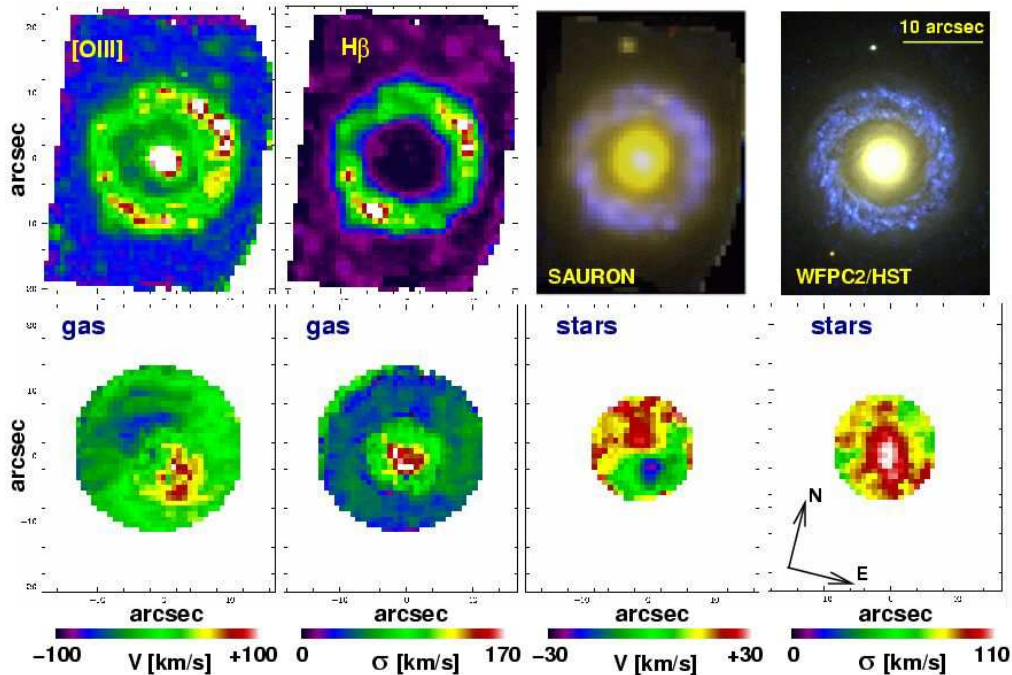


Figure 4. SAURON measurements of the stars and gas in NGC 7742, based on one pointing with seeing $1.5\text{--}2''.5$. The top row shows the emission-line intensity distributions of [OIII] and $H\beta$, followed by a reconstructed image composed of [OIII] and stellar continuum and a similar HST/WFPC2 image composed of F336W, F555W, and F814W exposures. The bottom row shows the derived gas velocity and velocity dispersion fields, followed by the stellar velocity and velocity dispersion.

5.2. NGC 4278

NGC 4278 is an E1-2 galaxy ($M_B = -19.9$) located in the Virgo cluster. It contains large-scale dust, as well as a blue central point source (Carollo et al. 1997). Long-slit spectroscopy reveals a peculiar stellar rotation curve, rising rapidly at small distances from the nucleus and dropping to nearly zero beyond $\approx 30''$ (Davies & Birkinshaw 1988; van der Marel & Franx 1993). NGC 4278 also contains a massive HI disk extending beyond $10 R_e$. The HI velocity field is regular but has non-perpendicular kinematic axes, indicating non-circular motions (Raimond et al 1981; Lees 1992).

Figure 5 displays the reconstructed stellar intensity as well as the [OIII] map derived from two SAURON pointings. Despite the regular and well-aligned stellar isophotes, the distribution of ionized gas is very extended and strongly non-axisymmetric. Its shape is reminiscent of a bar terminated by ansae, as observed in spiral galaxies. It will be interesting to construct a comprehensive dynamical model for NGC 4278, and explore its orbital structure and dark matter content.

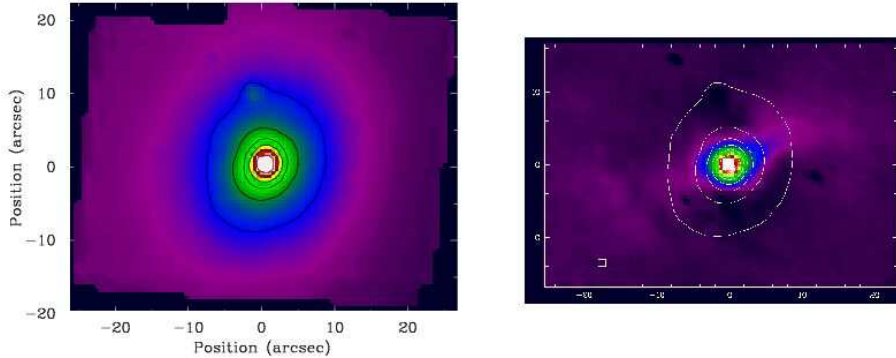


Figure 5. SAURON measurements of the stars and gas in NGC 4278, based on two partially overlapping pointings. The reconstructed stellar intensity is shown on the left and the [OIII] intensity on the right. Isophotes are overlaid on both images. The scales are identical but the fields-of-view differ slightly. The projected size of a SAURON lenslet is indicated in the bottom left corner of the second image.

6. Stellar Populations

SAURON’s wavelength range allows two-dimensional mapping of the line-strength indices $H\beta$, $Mg\ b$, and $Fe5270$. To convert measured equivalent widths to indices on the Lick/IDS system (Worthey et al. 1994), corrections for the difference in spectral resolution and velocity broadening in the galaxies must be applied. Both are described in Paper II. With stellar population models, these indices can be used to estimate luminosity-weighted ages and metallicities and study their contours. We discuss below the stellar populations of galaxies with kinematically decoupled cores. NGC 3384 shows a similar behaviour (Paper II).

Davies et al. (2001) discussed the SAURON kinematics and line-strengths of the large E3 galaxy NGC 4365 ($M_B = -20.9$) in the Virgo cluster. While the center and main body of the galaxy are decoupled kinematically, both components show the same luminosity-weighted age (≈ 14 Gyr) and a smooth metallicity gradient is observed, suggesting formation through gas-rich mergers at high redshift.

6.1. NGC 5813

NGC 5813 is an E1–2 galaxy in the Virgo-Libra Cloud ($M_B = -21.0$). It is undetected in HI or CO but has an unresolved, weak central radio continuum source and emission-line ratios typical of LINERS (Birkinshaw & Davies 1985; Ho, Filippenko, & Sargent 1997). The ionized gas exhibits a complex filamentary structure most likely not (yet) in equilibrium (Caon et al. 2000; Paper II).

As illustrated in Figure 6, NGC 5813 harbours a kinematically decoupled core (see also Efstathiou, Ellis, & Carter 1982). While the body of the galaxy appears purely pressure supported, the center rotates rapidly around an axis tilted by $\approx 13^\circ$ from the photometric minor axis. As in NGC 4365, the $H\beta$ map is featureless, indicating a roughly constant luminosity-weighted age, but the $Mg\ b$ and $Fe5270$ maps show a steep central gradient, indicating a strong metallicity gradient (see also Gorgas, Efstathiou, & Aragon-Salamanca 1990).

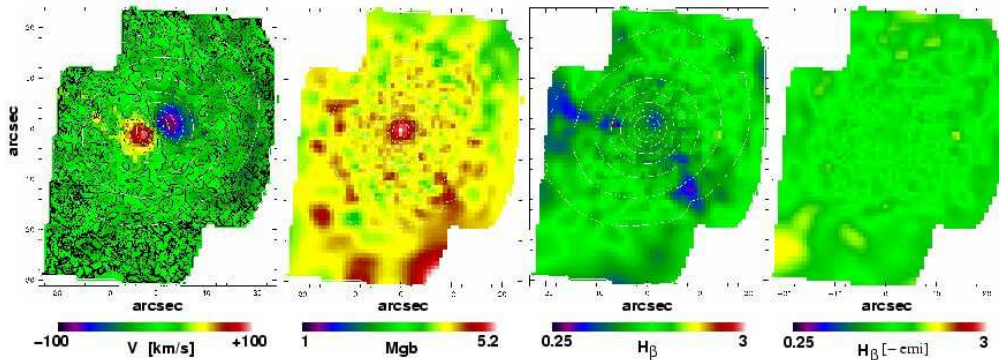


Figure 6. SAURON maps of NGC 5813, based on two partially overlapping pointings with seeing $1 - 2''.5$. From left to right: Stellar (mean) velocity field, Mg b map, raw $H\beta$ map, and $H\beta$ map corrected for emission. Isophotes are superposed on the first three images.

7. Concluding remarks

The SAURON survey will be completed in 2002. The first results show that early-type galaxies display line-strength distributions and kinematic structures which are more varied than often assumed. The sample contains specific examples of minor axis rotation, decoupled cores, central stellar disks, and non-axisymmetric and counter-rotating gaseous disks. The provisional indication is that only a small fraction of these galaxies can have axisymmetric intrinsic shapes.

We are complementing the SAURON maps with high-spatial-resolution spectroscopy of the nuclear regions using OASIS on the CFHT. STIS spectroscopy for many of the galaxies is in the HST archive. Radial velocities of planetary nebulae and/or globular clusters in the outer regions have been obtained for some of the galaxies, and many more will become available to $\approx 5R_e$ with a special-purpose instrument now under construction (Freeman et al. 2001, in prep).

Understanding the formation, structure, and evolution of galaxies is one of the central drivers in Ken Freeman's research. His enthusiasm and guidance at all levels is an inspiration to this entire field, and in particular to our team. We wish him and Margaret all the best for a happy and exciting future.

Acknowledgments. It is a pleasure to thank the ING staff for enthusiastic and competent support on La Palma. The SAURON project is made possible through grants 614.13.003 and 781.74.203 from ASTRON/NWO and financial contributions from the Institut National des Sciences de l'Univers, the Université Claude Bernard Lyon I, the universities of Durham and Leiden, the British Council, PPARC grant 'Extragalactic Astronomy & Cosmology at Durham 1998–2002', and the Netherlands Research School for Astronomy NOVA.

References

- Bacon R., et al. 1995, *A&AS*, 113, 347
Bacon R., et al. 2001, *MNRAS*, 326, 23 (Paper I)
Bender R. 1990, *A&A*, 229, 441
Bender R., & Nieto J.-L. 1990, *A&A*, 239, 97
Birkinshaw M., & Davies R.L. 1985, *ApJ*, 291, 32
Busarello G., Capaccioli M., D’Onofrio M., Longo G., Richter G., & Zaggia S. 1996, *A&A*, 314, 32
Caon N., Macchetto F.D., & Pastoriza M. 2000, *ApJS*, 127, 39
Carollo C.M., Franx M., Illingworth G.D., & Forbes D. 1997, *ApJ*, 710
Cretton N., Rix H.-W., & de Zeeuw P.T. 2000, *ApJS*, 536, 319
Davies R.L., & Birkinshaw M. 1988, *ApJS*, 68, 409
Davies R.L., Efstathiou G.P., Fall S.M., Illingworth G.D., & Schechter P.L. 1983, *ApJ*, 266, 41
Davies R.L., et al. 2001, *ApJ*, 548, L33
Davies R.L., Sadler E.M., & Peletier R.F. 1993, *MNRAS*, 262, 650
Dressler A. 1980, *ApJ*, 236, 351
Efstathiou G., Ellis R.S., & Carter D. 1982, *MNRAS*, 201, 975
Faber S.M., et al. 1997, *AJ*, 114, 1771
Ferrarese L., & Merritt D.R. 2000, *ApJ*, 539, L9
Fisher D. 1997, *AJ*, 113, 950
Gebhardt K., et al. 2000, *ApJ*, 539, L13
Gorgas J., Efstathiou G., & Aragon-Salamanca A. 1990, *MNRAS*, 245, 217
Gonzalez J.J. 1993, PhD Thesis, Univ. of California at Santa Cruz
Ho L.C., Filippenko A.V., & Sargent W.L.W. 1997, *ApJS*, 112, 315
Lees J.F. 1992, PhD Thesis, Princeton University
van der Marel R.P., & Franx M. 1993, *ApJ*, 407, 525
Mould J.R., Akeson R.L., Bothun G.D., Han M., Huchra J.P., Roth J., & Schommer R.A. 1993, *ApJ*, 409, 14
Peterson C.J. 1978, *ApJ*, 222, 84
Pogge R.W., & Eskridge P.B. 1993, *AJ*, 106, 1405
Raimond E., Faber S.M., Gallagher J.S., & Knapp G.R. 1981, *ApJ*, 246, 708
Roberts M., Hogg D., Bregman J., Forman W., & Jones C. 1991, *ApJS*, 75, 751
Rubin V.C., Kenney J.D.P., & Young J.S. 1997, *AJ*, 113, 1250
Sarzi M., et al. 2001, *ApJ*, 550, 65
Statler T.S. 1991, *ApJ*, 382, L11
Statler T.S. 1994, *AJ*, 108, 111
de Vaucouleurs G., & Buta R. 1980, *AJ*, 85, 637
Worthey G., Faber S.M., Gonzalez J.J., & Burstein D. 1994, *ApJS*, 94, 687
de Zeeuw P.T., et al. 2001, *MNRAS*, submitted (Paper II)
de Zeeuw P.T., & Franx M. 1991, *ARA&A*, 29, 239